Cu-NiO nano-composite formation through reactive milling: Reaction mechanism

Yasaman Kolvandi, Mohammad Aghagholizadeh, Saeed Sheibani*

School of Metallurgy and Materials Engineering, College of Engineering, University of Tehran, Tehran, Iran

*Corresponding author, Tel: 82084068; Fax: (+98) 21-88006076; E-mail: ssheibani@ut.ac.ir

Abstract

In this paper, the possibility of production of Cu matrix nano-composite powder containing 10, 37 and 54 wt.% NiO using mechano-chemical reduction of different copper oxides (CuO and Cu_2O) was studied. Structural evolutions were characterized by X-ray diffraction. Also, the microstructure was characterized by scanning electron microscopy and transmission electron microscopy. Particular attention has been paid to the reaction mechanism and kinetics using differential scanning calorimetry. It was found that the reactions completed gradually between 5 to 22h of milling. Formation of Cu_2O and Cu(Ni) solid solution, as intermediate phases, were observed during the reaction. It was found that, the initial excess Cu delayed reduction reaction and decreased the final crystallite size up to 18nm. Microstructural results showed that relatively large nano-composite agglomerates powder composed of uniform dispersion of NiO nano-particles in nano-crystalline Cu matrix were obtained. Kinetic study revealed that CuO reduction to Cu through two-steps reaction with lower activation energies in each step had higher rate, compared to one-step reduction of Cu_2O. Copyright © 2016 VBRI Press.

Keywords: Nano-composite, copper, mechano-chemical, mechanism.

Introduction

Copper matrix composites have been widely used in electronic packaging or manufacturing of electrodes and contact terminals due to both high strength and electrical conductivity. They can be synthesized by dispersing hard particles like oxides, carbides or nitrides into the copper matrix either by liquid or solid state techniques [1-3]. Favorable properties of Cu-NiO composite results in applications in different areas of science and industry such as electrochemical sensors [4-6], lithium ion batteries [7, 8] and transparent conducting oxide films [9].

Mechano-chemical processing, as a novel technique, has been gaining importance because of its potential applications for preparation of microcrystalline and nano-crystalline materials. In mechano-chemical method, powder particles are subjected to severe mechanical deformation during collisions with balls and vial and are repeatedly deformed, cold welded, and fractured, so that solid-state reactions in powder blends can be generate [10]. The reaction induced by high energy ball milling between copper oxides and different reductants such as Fe, Al, C, Ti, and Ca has been already investigated [11, 12]. Their products were often the mixture of copper with dispersed oxides particles, i.e. copper matrix composites. When this process was combined with mechanical milling, nano-structured composites with uniform distribution of reinforcement particles were synthesized. Few studies have been directed towards the mechano-chemical reaction between CuO and Ni [12]. However, the mechanism of different copper oxides (CuO and Cu_2O) reduction by Ni has not yet been thoroughly studied using thermal analysis. In the present work, the formation of Cu-NiO nano-composite powder was investigated through the reaction of different copper oxides of CuO and Cu_2O with Ni as follows.

$$Cu_2O_{(s)} + Ni_{(s)} \rightarrow 2Cu_{(s)} + NiO_{(s)},$$
$$\Delta G = -64894 + 16.4TlogT - 38.2T \quad J/mol \quad (1)$$
$$CuO_{(s)} + Ni_{(s)} \rightarrow Cu_{(s)} + NiO_{(s)},$$
$$\Delta G = -76505 + 20.9TlogT - 69.2T \quad J/mol \quad (2)$$
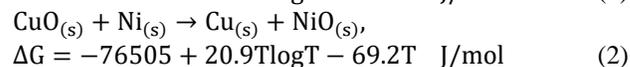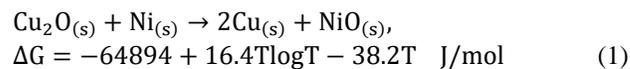
The thermodynamic data were taken from Gaskell [13]. Excess Cu powder would be added as a diluent and thermal conductor to help remove heat from the system during milling with the aim of a less violent reaction and controlling NiO content in Cu matrix. Particular attention was paid to the mechanism of this process via structural and microstructural variation during the mechanical milling. Knowledge of reactions mechanism make it possible to control the process under defined conditions.

Experimental

The initial powder materials were CuO (99%, <40 μm), Cu_2O (99%, <30 μm), Ni (99%, <1 μm) and Cu (99%, <75 μm). Two approaches were investigated: First, the powders mixture of the Cu_2O-Ni (called hereafter M1 sample) and CuO-Ni (called hereafter M2 sample) were milled corresponding to the stoichiometry of the reactions 1 and 2. Therefore, Cu-37%wt. NiO and Cu-54%wt. NiO nano-composite powders were produced based on stoichiometry of the reactions 1 and 2, respectively.

Second, for producing a Cu-10%wt. NiO nano-composite powder, excess Cu powder was added to initial powder mixtures corresponding to the nominal content of 10 %wt. NiO in the final product. In fact, the powders mixture of Cu_2O-Ni-Cu (called hereafter CM1 sample) and CuO-Ni-Cu (called hereafter CM2 sample) were milled. A 10 gr of initial powder mixtures were charged into a hardened steel vial with hardened steel balls and then milled in a high energy planetary ball mill (PM2400) under argon atmosphere. The ball to powder ratio and rotation speed were 25:1 and 300 rpm, respectively.

The investigation for phase identification accomplished using X-ray diffraction (XRD) (Philips PW 3040/60) with a radiation of Cu Kα. The line broadening due to the instrument was calculated from Warren's method [14]. The mean crystallite size was obtained using Williamson-Hall plot [15]. The lattice parameters were calculated from XRD data [16]. Also, the morphological analysis of particles was inquired by a field emission scanning electron microscope (FESEM) (Hitachi S4160 at an accelerating voltage of 5 kV). To prepare the FESEM sample, the powder is mounted on an aluminum stub with adhesive, coated with Gold. In addition, transmission electron microscopy (TEM) (Philips EM208S, operated at 100 kV) was used to study the microstructure in more details. To prepare the TEM sample, the sample was dispersed in ethanol through an ultrasonication process, and then a drop of the dispersion was placed on a copper grid coated with carbon film, which was dried naturally at room temperature.

Differential scanning calorimetry (DSC) experiments were performed in a SDT Q600 instrument and argon gas flow of 100 ml/min was applied during the measurement. All experiments were carried out on samples in standard platinum pans, with an empty pan as the standard. The measurements were performed at four different heating rates, *i.e.* 5, 10, 15 and 20 K/min. Once the samples were cooled down to room temperature, a second set of DSC curves was recorded at the same heating rates previously used for recording the corresponding DSC curves of the first set to be used as base line. A precise measure of the heat flow can thus be obtained by measuring and integrating the difference between the first and second scans.

Results and discussion

Structural results

Fig. 1 shows XRD patterns of M1 and CM1 samples after different milling times. The progress of mechano-chemical reduction of Cu_2O by Ni in M1 sample was shown in **Fig. 1 (a)**. The intensity of XRD peaks corresponding to the Cu_2O has been observed to decrease by milling. However, no additional peaks corresponding to any new phase have been observed up to 2h. During the following 3h of milling, Cu and NiO peaks appeared in the XRD pattern and Cu_2O peaks almost disappeared, as shown in **Fig. 1 (a)**. After 7 hours of milling, all the initial Cu_2O and Ni powders were consumed and the resulting powder consisted of only the Cu and NiO phases. It should be noted that the peak intensities of Cu(111), 2θ of 43.32 degree, and NiO (400), 2θ of 43.29 degree, were

most intense in XRD patterns. However, due to peak broadening at long milling times, these peaks tend to overlap. Therefore, the NiO (222), 2θ of 37.26 degree, was analyzed instead as a formation of NiO phase criterion. **Fig. 1 (b)** represents the mechano-chemical reduction of Cu_2O by Ni in presence of excess Cu in CM1 sample. The diffraction peaks of Ni cannot be detected in XRD patterns is probably due to its small quantity. With longer milling time, the peaks of Cu became broader and Cu_2O peak intensities decreased. After 22h of milling, the Cu_2O peaks disappeared completely, and only the peaks corresponding to Cu and NiO were observed. Hence, the reaction completed gradually within 22h of milling. This is due to the presence of Cu powder in CM1 sample which delays the reaction between Cu_2O and Ni. Thus, the time for the overall reaction 1 in CM1 is 22h, which is longer than that in the M1 sample. The delay in reaction during mechano-chemical synthesis due to matrix metal has been also reported in literatures [17, 18].
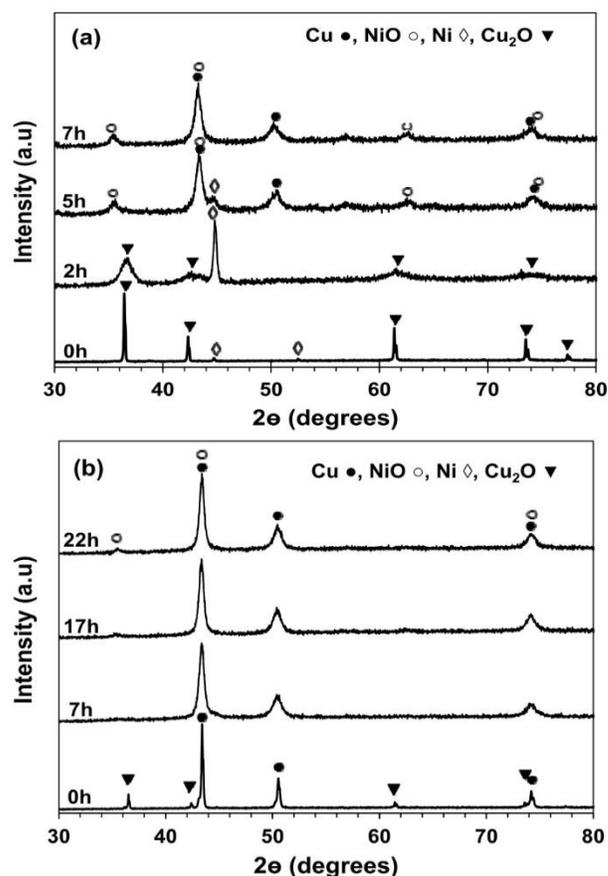
Fig. 1. XRD patterns of (a) M1 and (b) CM1 samples as a function of milling times.

Fig. 2 shows XRD patterns of M2 and CM2 samples after different milling times. It represents the progress of mechano-chemical reduction of CuO by Ni during the milling process. Similar to that observed in M1 and CM1 samples, all the peaks tend to broaden as the milling time increases and their intensities decrease. It can be found in **Fig. 2 (a)** that almost all CuO peaks disappeared after milling for 1h which is probably due to the CuO amorphization [10]. The Cu and NiO peaks appeared with

increased milling time up to 1.5h. It should be noted that, the appearance of Cu_2O phase after 1.5h of milling was an indication of intermediate phase formation. However, Cu_2O peaks was gradually disappeared after 3h of milling. Finally, the mechano-chemical reaction completed gradually after 5h. **Fig. 2 (b)** represents the mechano-chemical reduction of CuO by Ni in presence of excess Cu in CM2 sample. It can be seen that the reaction completed gradually within 20 hours of milling. It is obvious that formation of Cu and NiO phases was postponed by adding excess Cu powder to the starting materials, which agrees very well with the results of CM1 sample (**Fig. 1(b)**). Unlike the M2 sample, no peak related to the formation of Cu_2O as the intermediate phase was observed. The reason possibly being the gradual formation of Cu_2O. Hence this phase was not detectable in the XRD pattern (**Fig. 2(b)**) which was probably due to its small quantity and its high dispersion.
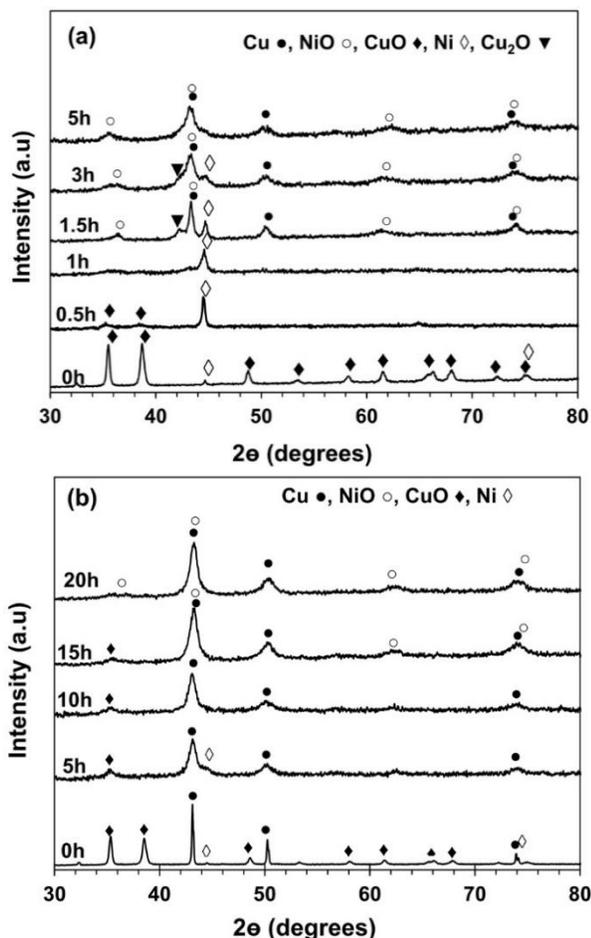
Fig. 2. XRD patterns of (a) M2 and (b) CM2 samples as a function of milling times.

Munir [**19**], proposed that the value of adiabatic temperature can be used as a rough guide to the existence of combustion or progressive reaction in the milling process. It means that the adiabatic temperature, which is the maximum temperature achieved under adiabatic conditions as a consequence of the evolution of heat from the reaction, should be above 1800 K, in combustion reactions. The calculated adiabatic temperature of reactions 1 and 2 were 711 and 1288 K, respectively.

Therefore, both reactions progressed gradually with milling time. This is consistent with low enthalpy of the reactions and gradual mechano-chemical reduction of copper oxides by Ni observed in XRD results (**Fig. 1** and **2**).

Moreover, the XRD patterns (**Fig. 1** and **2**) exhibit the broadening increases with milling time. This is due to the decrease in the crystallite size and an increase in internal lattice strains. These defects can provide a driving force for solid-state reaction during ball milling [**10**]. The mean crystallite sizes of all prepared samples calculated from XRD patterns are shown in **Fig. 3.** It can found that longer milling times in M1 and CM1 samples than that of M2 and CM2 samples lead to decrease in final crystallite size. Furthermore, the smaller crystallite sizes in CM1 and CM2 samples suggest higher microstructural refinement of excess Cu which was added from initial stage of milling operation. It should be noted that, the error bars represent the accuracy of determination of crystallite size from XRD patterns.
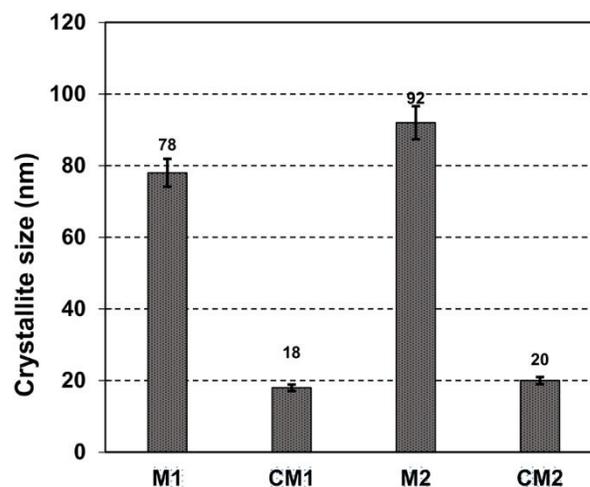
Fig. 3. Cu crystallite size of final product from different M1, CM1, M2 and CM2 samples.

For further details on the structural evolution during milling, Cu lattice parameter changes were calculated from shifts in peak positions in XRD patterns. Since the intensity of Cu peaks were very small for M1 sample milled for 2h, the Cu lattice parameter could be calculated after 5h milling (see **Fig. 4 (a)**). Similarly for M2 sample, the Cu peaks intensities were not sufficiently high until 1.5h and therefore, the extraction of lattice parameter was not accurate before that. **Fig. 4 (a)** shows the Cu lattice parameter changes during milling of M1 and CM1 samples. It can be seen that Cu lattice parameter after 5h milling in M1 sample was 0.3601 nm. After 7h of milling, the value of lattice parameter increased to 0.3615nm which was equal to that of theoretical value of pure Cu [**20**]. Furthermore, that same trend in lattice parameter change can be observed in **Fig**. **4 (a)** and **(b),** for three other samples (CM1, M2 and CM2). The lattice parameter of Cu decreased initially and reached a minimum value then it increased at longer milling times. The reduction of lattice parameter is possibly attributed to Cu(Ni) solid solution formation. As nickel's atomic radius (1.2459 nm)

is smaller than that of copper (1.2780 nm), the solid solution formation causes a decrease in lattice parameter [20]. Similar observation has also been reported previously during mechanical alloying in a Cu-Ni system [21]. However, the increase of the Cu lattice parameter at longer milling times may be related to the NiO phase formation by further reactions. In fact, when this phase forms, Ni solute atoms are driven out of the solid solution. It can be concluded that the Cu(Ni) solid solution appeared as intermediate phase during the milling process.
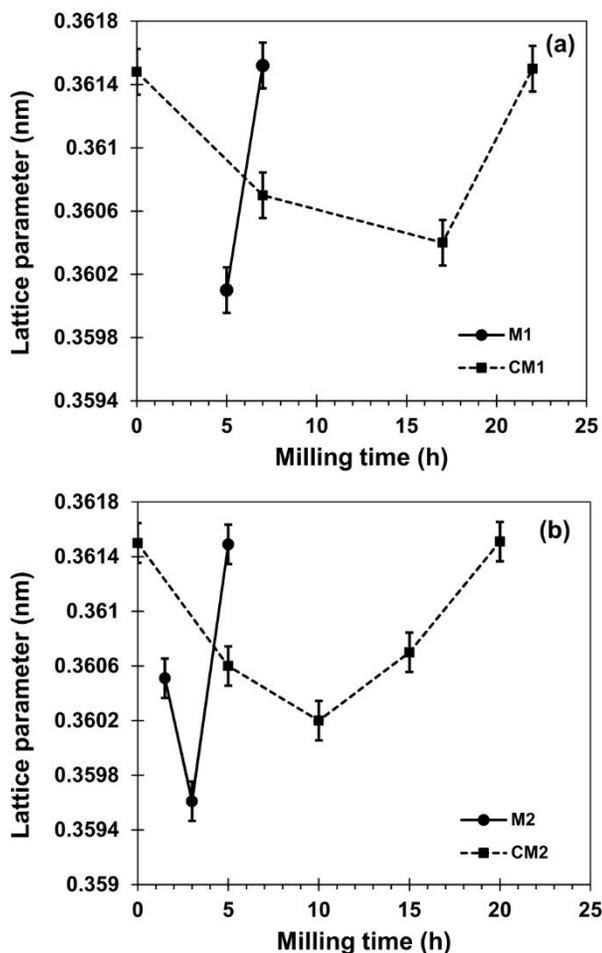
Fig. 4. Cu lattice parameter changes as a function of milling time for (a) M1 and CM1 and (b) M2 and CM2 samples.

All the above structural results suggest that Cu_2O and Cu(Ni) solid solution appear as intermediate phases during the milling process of M2 sample, suggesting that the reaction progresses gradually. Hence, the following sequence may be assumed for CuO mechano-chemical reduction through reaction 2:

$$CuO + Ni \xrightarrow{1.5 \text{ h milling}} Cu_2O + Cu(Ni) + NiO \xrightarrow{3.5 \text{ h milling}} Cu + NiO \quad (3)$$
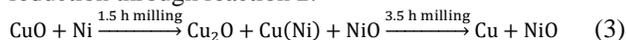
DSC results

In order to get a better understanding of the reactions mechanism, M1 and M2 as-mixed powders were investigated by DSC analysis. **Fig. 5** shows the DSC scans of as-mixed M1 and M2 powders. As shown in **Fig. 5 (a)**, M1 as-mixed powder showed only an

exothermic peak. However, in DSC trace of M2 as-mixed powder in **Fig. 5 (b)**, two exothermic reactions occurred. In order to investigate the origin of the exothermic peaks in each sample, the as-mixed M1 and M2 powders were heated to the selected temperatures in the vicinity of exothermic peaks in DSC curves, cooled to room temperature, and examined by XRD. It should be noted that XRD patterns are skipped here. The large exothermic peak in as-mixed M1 powder (**Fig. 5 (a)**) resulted from the formation of Cu through of reaction 1. On the other hand, the first small peak in as-mixed M2 powder (**Fig. 5 (b)**) is probably attributed to the reduction of CuO to Cu_2O by Ni. Also, the larger one is ascribed to the reduction of Cu_2O by Ni and Cu formation.
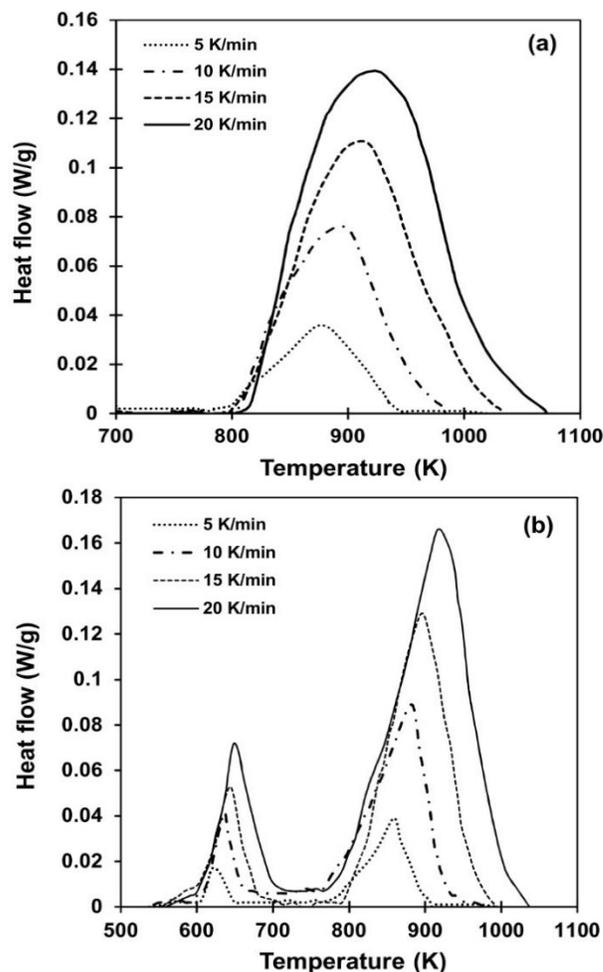
Fig. 5. DSC results of as-mixed (a) M1 and (b) M2 powders at different heating rates of 5, 10, 15, 20 K/min.

The enthalpy associated with the exothermic peaks ($\Delta H_{experimental}$) was calculated from the integration of the overall DSC curves which are summarized in **Table 1**. On the other hand, theoretical exothermic thermal effects ($\Delta H_{theoretical}$) [13] accompanying with the reactions are summarized in **Table 1**. A quantitative agreement of the heat release during reactions with the theoretical enthalpy is observed. This agreement is particularly remarkable in view of the fact that the exothermic peak in M1 sample is related to reaction 1. In addition, overall first and second peaks in M2 sample are related to the reaction 2. The first peak in DSC scan of M2 sample is related to the reduction

of CuO to Cu_2O by Ni, and the second peak is related to the reduction of Cu_2O to Cu by Ni. This also confirms the proposed sequence of CuO to Cu conversion during ball milling (Eq. 3).

Table 1. Enthalpy changes, activation energy and Suggested reaction for different samples.

Sample	$\Delta H_{experimental}$ (kJ/mol)	$\Delta H_{theoretical}$ (kJ/mol)	E (kJ/mol)	Suggested reaction
M1	62.5 ± 4.12	66.50	215 ± 8	$Cu_2O + Ni \rightarrow 2Cu + NiO$
M2 (overall)	74.37 ± 3.57	77.80	-	$CuO + Ni \rightarrow Cu + NiO$
first peak	10.27 ± 3.89	11.30	150 ± 6	$2CuO + Ni \rightarrow Cu_2O + NiO$
second peak	64.10 ± 3.25	66.50	173 ± 4	$Cu_2O + Ni \rightarrow 2Cu + NiO$

In order to compare the kinetics of copper oxides reduction through reaction 1 and 2 in more detail, activation energies, E, were calculated. Calculation of E was based on a multiple scan method in which several measurements performed at different heating rates. This value has been determined from the isoconversional Kissinger equation [22], and summarized with suggested related reactions in **Table 1**. In summary, three conclusions could be drawn as follows.

The first step of two-steps reaction 2 in M2 sample has lower activation energy and hence higher rate than that of the second step. This is in accordance with milling results. As stated in the suggested mechanism in Eq. 3, the first and second reaction steps were occurred after 1.5 and 3.5h of milling, respectively.

The activation energies in each steps of two-steps reaction 2 in M2 sample are lower than that of reaction 1 in M1 sample. It means higher rate of reaction in M2 sample. This result is in good agreement with the reactions progress through mechanical milling. By the comparison of **Fig**. 1 (a) and **Fig. 2 (a)**, it can be found that the reactions 1 and 2 were completed after 7 and 5h of milling, respectively. This can be explained by the fact that the rate of overall reaction 2 is the rate of the slowest step [23]. It means that the rate determining step in M2 sample is second step which has lower activation energy than that of reaction in M1 sample.

Actually, DSC peak in M1 sample and second DSC peak in M2 sample are related to reaction 1. By the comparison of calculated activation energies from these two peaks, it can be found that the activation energy of Cu_2O reduction to Cu in M1 sample decreases from 215 to 173 kJ/mol in M2 sample. This result can explain the higher rate of Cu_2O reduction to Cu in M2 sample. By the comparison of **Fig. 1 (a)** and **Fig. 2 (a)**, it can be found that this reaction completed after 7 and 3.5h of milling in M1 and M2 samples, respectively. The reason for this appears to be the heat emission caused by the first step in M2 sample. It could be stated that the heat initiates and accelerates the second step. Another possible reason is that, the produced intermediate Cu_2O in M2 sample through milling process was more activated than initial Cu_2O in M1 sample. It facilitates the course of Cu_2O reduction by Ni in M2 sample.

Microstructural results

Fig. 6 shows FESEM images of final nano-composite products produced from different samples. It can be seen

that the produced nano-composite powders from M1 and M2 samples (see **Fig. 6 (a)** and **(c)**) have irregular shape with loosely agglomerated state. FESEM images at higher magnification (inset of **Fig. 6 (a)** and **(c)**) show that nano-composite particles are mostly comprised of fine primitive nano-particles. It can be seen from **Fig. 6 (b)** and **(d)** that the addition of excess Cu to the initial powder mixture in CM1 and CM2 samples forms a relatively coarse agglomerates. It is well known that face-centered-cubic (fcc) metals like Cu have a stronger tendency to form agglomerates during milling than other metals which are more brittle [10]. It can be found that powder particles reached a steady state with the average size of 50 μm.
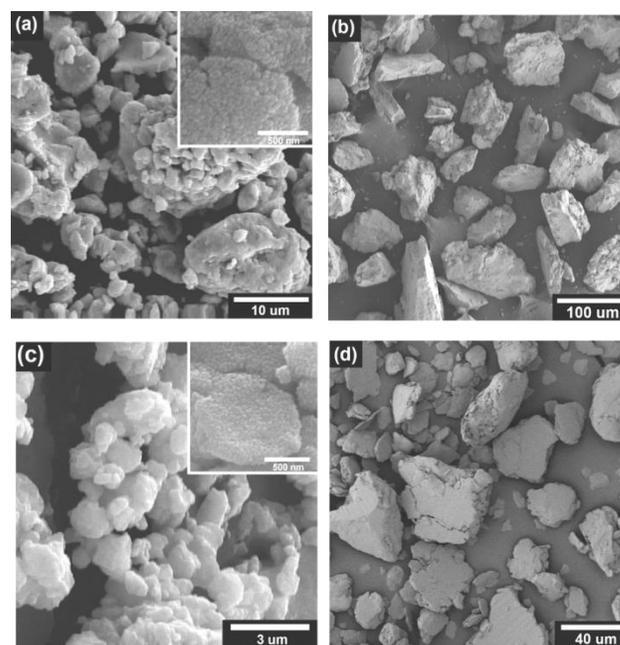
Fig. 6. FESEM images of (a) 7h milled M1, (b) 22h milled CM1, (c) 5h milled M2 and (d) 20h milled CM2 samples.

In order to get a better understanding of the Cu-NiO nano-composite formation, themicrostructure of 20h milled CM2 sample was investigated by TEM. Similar results were obtained for other compositions investigated and TEM images of other samples are skipped here. Typical bright and dark-field images with corresponding selected area diffraction (SAD) pattern (the bottom-left corner) are shown in **Fig. 7**. The bright-field TEM image in **Fig. 7 (a)** confirms a very fine nano-crystalline structure. The bright-field and dark field images show that all the crystallites have sizes of about 30 nm and less, which is also comparable with the results in **Fig**. 3, obtained from the XRD analysis. In TEM image, the grain boundaries are not easily detectable. This is mainly caused by the inhomogeneous contrast and indicates that a high level of internal lattice strain is present within the matrix [24]. This refined structure to nanometer scale is further evinced by the continuous circular SAD pattern inset in **Fig. 7 (b)**. Rings corresponding to both Cu and NiO phases are exhibited in this figure. It is evident in dark field image (**Fig. 7 (a)**) that a composite with nano-scale NiO particles homogeneously distributed in the copper matrix was prepared.
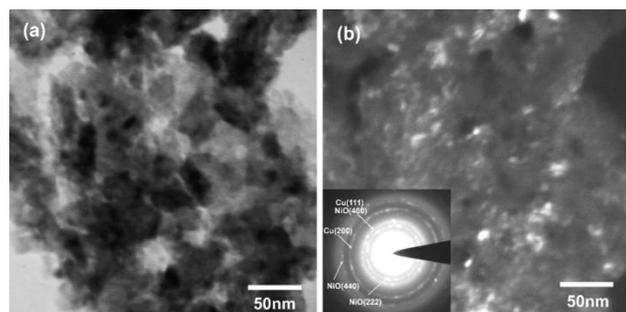
Fig. 7. TEM images of CM2 sample after 20h milling: (a) bright-field image and (b) dark-field image obtained using (222).

Conclusion

In this study, Cu-NiO nano-composite was produced by mechano-chemical reduction of CuO and Cu_2O by Ni using high energy ball milling. Also the effect of excess initial Cu powder on the reaction progress was investigated to produce Cu-10%wt NiO nano-composite. Phase evolutions of the milled powders revealed that the reaction progressed gradually with milling time. In the case of Cu_2O reduction, Cu(Al) solid solution as an intermediate product was formed. In the case of CuO reduction, formation of Cu(Al) solid solution and Cu_2O phase as the intermediate products were found, as well. The results showed that, initial excess Cu delayed the mechano-chemical reduction of CuO and Cu_2O with Ni. Hence, final nano-composites showed smaller crystallite sizes in presence of initial excess Cu powder, because of longer milling times. Additionally, the mechanism and kinetics of Cu-NiO formation were explained by DSC analysis. Reduction of CuO to Cu through two-steps reaction with lower activation energies in each step had higher rate, compared to one-step reduction of Cu_2O. Also, Cu_2O reduction by Ni was accelerated during two-steps reaction in comparison with one-step reduction reaction. Furthermore, FESEM results indicated that Cu-NiO nano-composite powders had relatively irregular shape consisted of ultra fine particles. However, relatively coarse agglomerates of nano-composite powders were produced in presence of excess initial Cu powder. Also, TEM results showed that NiO nano-particles distributed in the nano-crystalline copper matrix, which agrees well with the XRD results.

References

1. Tjong, S.C.; Lau, K.C; *Mater. Sci. Eng. A*, **2000**, *282*, 183.
   DOI: 10.1016/S0921-5093(99)00752-2
2. Kumari, S.; Kumar, A.; Sengupta, P.R.; Dutta, P.K.; Mathur, R.B; *Adv. Matter. Lett.*, **2014**, *5*, 265.
   DOI: 10.5185/amlett.2013.10546
3. Kulthe M.G.; Goyal, R.K; *Adv. Matter. Lett.*, **2012**, *3*, 246
   DOI: 10.5185/amlett.2012.3326
4. Fang, B.; Gu, A.X.; Wang, G.F.; Wan g, W.; Zhang, C.H.; Feng, Y.H.; Zhang, X.J; *ACS Appl. Mater. Interfaces,* **2009**, *1*, 2829.
   DOI: 10.1021/am900576z.
5. Wang, G.F.; Gu, A.X.; Wang, W.; Wei, Y.; Wu, J.J.; Wang, G.Z.; Zhang X.J.; Fang, B; *Electrochem. Commun.,* **2009**, *11*, 631.
   DOI: 10.1016/j.elecom.2008.12.061
6. Zhang, X.; Gu, A.; Wang, G.; Huang, Y.; Ji, H.; Fang, B; *Analyst*, **2011**, *136*, 5175.
   DOI: 10.1039/C1AN15784A
7. Chen, H.; Li, C.; Li, N.; Xiang, K.; Hu, Z; *Micro & Nano Letters*, **2013**, *8*, 544.
   DOI: 10.1049/mnl.2013.0330
8. Abbas, S.M.; Hussain, S.T.; Ali, S.; Ahmad, N.; Ali, N.; Abbas, S.; Ali, Z; *J. Solid State Chem.*, **2013**, *202*, 43.
   DOI: 10.1016/j.jssc.2013.03.036
9. Chen, S.C.; Kuo, T.Y.; Lin, Y.C.; Lin, H.C; *Thin Solid Films*, **2011**, *519*, 4944.
   DOI: 10.1016/j.tsf.2011.01.058
10. Suryanarayana, C; *Prog. Mater. Sci.,* **2001**, *46*, 1.
    DOI: 10.1016/S0079-6425(99)00010-9
11. Schaffer, G.B.; McCormick, P.G; *Metall. Trans. A*, **1991**, *22*, 3019.
    DOI: 10.1007/BF02650262
12. Schaffer, G.B.; McCormick, P.G; *Metall. Trans. A*, **1990**, *21*, 2789.
    DOI: 10.1007/BF02646073
13. Gaskell D.R.; Introduction to Metallurgical Thermodynamics; 3rd ed., McGraw-Hill: New York, NY, **1981**.
14. Cullity, B.D.; Stock, S.R.; Elements of X-ray Diffraction. 3rd ed., Prentice Hall: Upper Saddle River, NJ, **2001**.
15. Williamson, G.K.; Hall, W.H; *Acta Metall.*, **1953**, *1*, 22.
    DOI: 10.1016/0001-6160(53)90006-6
16. Correia, J.; Davies, H.; Sellars, C; *J. Acta Mater.*, **1997**, *45*, 177.
    DOI: 10.1016/S1359-6454(96)00142-5
17. Zhou, L.Z.; Guo, J.T.; Fan, G.J; *Mater. Sci. Eng. A*, **1998**, *249*, 103.
    DOI: 10.1016/S0921-5093(98)00576-0
18. Fan, G.J.; Quan, M.X.; Hu, Z.Q.; Eckert, J.; Schultz L; *Scripta Mater.* **1999**, *41*, 1147.
    DOI: 10.1016/S1359-6462(99)00285-7
19. Munir, Z.A.; Anselmi-Tamburini, U; *Mater. Sci. Rep.,* **1989**, *3*, 279.
    DOI: 10.1016/S0920-2307(89)80002-7
20. Lubarda, V.A; *Mech. Mater.,* **2003**, *35*, 53.
    DOI: 10.1016/S0167-6636(02)00196-5
21. Ban, I.; Stergar, J.; Drofenik, M.; Ferk, G.; Makovec, D; *J. Magn. Magn. Mater.*, **2011**, *323*, 2254.
    DOI: 10.1016/j.jmmm.2011.04.004
22. Kissinger, H.E; *Anal. Chem.,* **1957**, *29,* 1702.
    DOI: 10.1021/ac60131a045
23. Levenspiel O.; Chemical Reaction Engineering, 2nd ed., John Wiley and Sons: New York, **1999**.
24. Botcharova, E.; Freudenberger, J.; Gaganov, A.; Khlopkov, K.; Schultz, L; *Mater. Sci. Eng. A*, **2006**, *416,* 261.
    DOI: 10.1016/j.msea.2005.10.022